

## T9 Analysis of errors in measurements and inversion

Philippe Le Masson<sup>1</sup>, Morgan Dal<sup>2</sup>, Thomas Pierre<sup>1</sup>

<sup>1</sup>Laboratory of LIMATB, University of South Brittany/ European University of Brittany, Research center, (rue de saint maude, 56321 Lorient Cedex)

<sup>2</sup>Laboratory PIMM, Arts et Métiers, Paris Tech, 151 Bd. de l'Hôpital, 75013 Paris

[philippe.le-masson@univ-ubs.fr](mailto:philippe.le-masson@univ-ubs.fr), [morgan.dal@ensam.eu](mailto:morgan.dal@ensam.eu), [thomas.pierre@univ-ubs.fr](mailto:thomas.pierre@univ-ubs.fr)

**Abstract:** This workshop seeks to focus on two objectives. the first objective aims to develop an estimation and is based on two software. Comsol Multiphysics is a computer code to simulate different types of physical equations. Moreover, it offers the possibility to save the steps of numerical development to be able to then work on one or more parameters. Matlab helps develop the estimation algorithms and allows the use of the direct problem developed under COMSOL and modification of the parameter to be estimated. The second objective aims to study the measurement errors associated with the intrusive aspect of thermocouples. Several configurations of instrumentation are reviewed and then by making estimates with wrong data measurements, analyze the errors in the estimated values.

### 9.1 Introduction

The difficulty every researcher wishing to approach a physical phenomenon meets is choosing the model which best corresponds to reality. For that purpose, knowledge of the parameters and/or the functions of the modelling is imperative. These data can be, indeed, obtained in the literature but also by an approach of the inverse techniques. In an inverse problem, we have information (measures of temperatures, heat flux, deformations...) which are the effects of the causes we try to estimate. It is, thus, a question of identifying the laws of the physics that we study. Although the inverse techniques apply to all the domains of physics, we shall limit ourselves to the problems of heat diffusion

In this tutorial, we shall particularly emphasize the quality of the measures that it is constantly necessary to try to obtain. Figure n°1 of the course of the METTI [1], summarizes the usually followed inverse and direct approaches. We find five types of estimation errors there. If we do not take the effects of coupling between these various terms into account, the global error can be defined as the sum of these types of errors:

$$e_g = e_1 + e_2 + e_3 + e_4 + e_5 \quad (9.1)$$

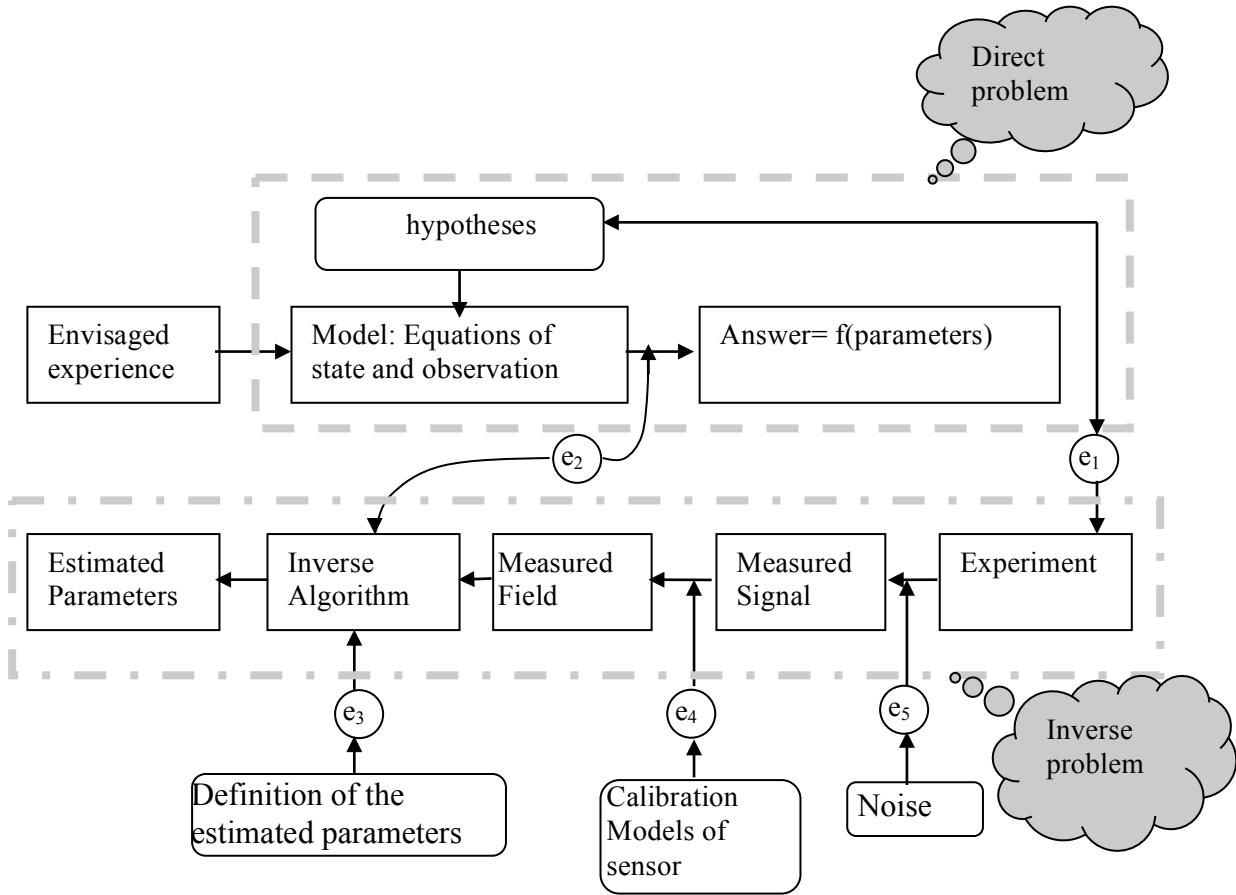


**Figure 1: Summary of the inverse and direct approaches**

The direct problem is only a mathematical image of our experiment. If the hypotheses made for the definition of this problem are too far away from the experiment, an error  $e_1$  can lead us towards a not realistic estimation. Furthermore, the resolution of the direct problem appeals to various methods. The calculated answer is more or less different from the exact answer required by the model. The errors of resolution (error of numerical scheme connected to the steps of time, to the steps of space, as well as to the precision of the computer ...) are going to lead to an error  $e_2$  of estimation.

These first two errors are generally met during the modelling of a phenomenon for which we do not completely know the physics, in particular in the case of coupling between several domains (heat conduction - electricity - phase change...).

To these errors will eventually be added other errors for the inverse problems:

First of all, the error  $e_3$  is an error resulting from objectives of the experiment reverser.

The composed questions are:

- ✓ Do we have some knowledge of the shape of the law which we want to estimate?
- ✓ Have we worked on the estimation of a perfectly unknown function or have we estimated the parameters of a law?
- ✓ What is the spatial and/or temporal domain on which we have to estimate our parameters and/or our functions?
- ✓ In the case of an estimation on a limited domain, what are the parameter values for the rest of the domain?

- ✓ What are the errors on the estimation owed to the uncertainties connected to the knowledge of the known data (for example: spatiotemporal data: position of the sensors, the measures of the forms of the sample)?

Having partly answered these questions by the choice of a parameterization of the function that we want to estimate, by the study of the sensitivity coefficients when faced with the position of the sensors and the uncertainties on the known data, the error is stressed by the fact that the inverse methods themselves produce errors on estimated values. These last errors are engendered by the method.

The fourth component  $e_4$  of the error of the estimation results from the conversion of the signal delivered by the sensor in size of the same physical dimension as the field solution of the direct problem (temperature for example). It is thus connected to the characteristics of the sensor (problems of the non linearity of the sensor, the reproducibility of a measure...) and results from the definition of the experimental design of these sensors in the experiment (intrusive character of the sensor). The study of these errors of thermal metrology is an important element to obtain a quality estimation.

The last of the estimation errors  $e_5$  is due to the measuring device of the signal produced by the sensor. This error can be defined under the general term of "noise". J.V. Beck and K.J. Arnold [2] presented hypotheses on the nature of this noise allowing for the implementation of the methods of estimation.

- ✓The noise is additif:

$$Y_i = T_i + \varepsilon_i \quad (9.2)$$

where  $Y_i$  is the measured temperature,  $T_i$  is the exact temperature and  $\varepsilon_i$  a random noise

- ✓The noise  $\varepsilon_i$  has a mean value:

$$E(\varepsilon_i) = 0 \quad (9.3)$$

- ✓The noises associated to the various measures are not correlated. Two noises of measures  $\varepsilon_i$  and  $\varepsilon_j$  are said non-correlated if their covariance verifies:

$$\text{cov}(\varepsilon_i, \varepsilon_j) \equiv E[(\varepsilon_i - E(\varepsilon_i))(\varepsilon_j - E(\varepsilon_j))] = 0, \text{ for } i \neq j \quad (9.4)$$

In this case, the noise  $\varepsilon_i$  has no effect on and no relation with the noise  $\varepsilon_j$

- ✓The noise has a constant standard deviation:

$$\sigma_i = \sqrt{E\left[\left[Y_i - E(Y_i)\right]^2\right]} = \text{const.} \quad (9.5)$$

- ✓The considered noise follows a normal probability distribution.
- ✓We incline no information in priori about the unknown to estimate
- ✓Only the measures used in the estimation procedure are noised. Other present parameters in the model are supposed to be exactly known.

These enumerated hypotheses are rarely combined in reality. They are emitted for the validity of the estimation methods.

In this course, we thus suggest analyzing the error  $e_4$ . We shall also try to make a link between the errors of measurement and the developed direct model by integrating into it the modelling of the sensor. Working mainly on the measurement of temperature by thermocouples, we shall have to take into account several special points such as the drilling of the sample, as well as the quality of the contact between the sensor and the sample.

## 9.2 Temperature measurement by thermocouple and errors of measurement

Any temperature measures by thermocouple on or in a sample generate errors of measure by its intrusive aspect. First of all, the temperature measure in a point of a material environment in fact involves a measure of a small element surrounding this point. Furthermore, when in the environment we have important gradients of temperature, we suppose that the element of volume is small enough so that the temperature is practically uniform. Finally, if the considered element is defined on the surface, it has to take into account the fact that the surface possesses specificities such as its roughness, its heterogeneousness connected, for example, to surface treatments (oxidation, quenching).... All these physical specificities underline the difficulties, on one hand, to integrate a sensor whose physical characteristics are often different from the environment where we want to realize the measure and, on the other hand, to estimate the disturbance which this sensor engenders.

In a general way, following the use of the sensor (strong temperature gradients or not, steady state or transient, strongly transient phenomenon or not), we have to master the parameters of implementation, namely, its calibration, its sensitivity as well as all the involved thermoelectric effects. Numerous works [1] [3] summarize these various aspects towards the size of the sensor, his presence on or in the sample and of the chain of measure.

In this course, we are mainly going to emphasize the presence of the sensor and the disturbance which it generates on the phenomena of the heat diffusion. In any theory, the presence of the sensor in an environment supposes a modification of the heat transfers by conduction, convection or radiation in the middle. The local temperature is modified. Concerning more particularly the surface temperature measure, the presence of a sensor modifies the emissivity and the exchanges by radiation. The sensor and the elements transferring the information (thermocouple wires, for example) are affected by the outside conditions, so provoking a measure which can be very different from the one to measure.

### 9.2.1 Error during a measure of a surface temperature.

As we were able to underline it above, during a measure of a surface temperature, the superficial exchanges are modified by the presence of the sensor and the thermophysic and radiative properties are different from the middle. Furthermore, because of the link between the sensor and the acquisition of measure, a parasite heat flux is passed on through it and then towards the environment. A generation or an absorption of heat at the level of the sensor can also occur. Furthermore, because of the methodology of the setting-up of the sensor, we can have an exothermic or endothermic reaction of chemical origin. All these heat transfers make a disturbance of the surface temperature.

The temperature is not  $T$  but  $T_p$ . Figure 2 presents the heat transfers during a measure of a surface temperature. We can note that in the presented case, because of a heat transfer from the material to the outside environment and thus the pumping of energy engendered by the sensor, the temperature  $T_p(t)$  is lower than the true temperature of the surface. Furthermore, generally the temperature sensor is implanted on the surface of the material with a contact that very often remains imperfect. The sensor is thus going to recover, in the case of Figure 2, an intermediate temperature noted  $T_c(t)$  defined between the new temperature of the surface  $T_p(t)$  and the temperature of the outside environment  $T_e(t)$ . So in the sensor, we have a parasite heat transfer, noted  $\varphi(t)$ . In reality, during this heat transfer, three effects conjugate:

- ✓ The first effect occurs in the material through the convergence of the lines of heat flux towards the sensor (macroconstriction effect).
- ✓ The second effect is connected to the quality of the contact between the sensor and the material. A contact resistance between both elements provokes a temperature drop in the interface.
- ✓ The third effect is laid to the exchanges between the sensor, the wires of the sensor and the ambient environment. This effect is also mentioned as the fin effect.

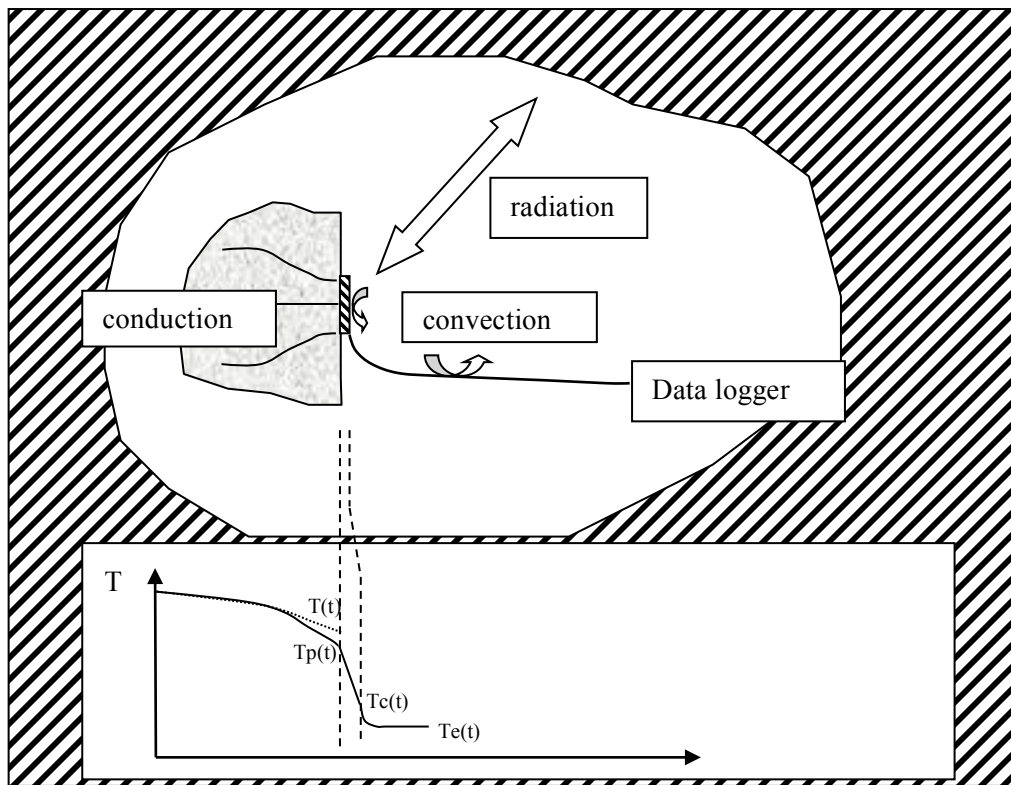


**Figure 2: heat Transfers through the surface sensor**

So as we were able to highlight above, a measure error appears and is represented by the distance between the true temperature  $T(t)$  and the temperature on the sensor  $T_c(t)$ :

$$\varepsilon(t) = T(t) - T_c(t) \quad (9.6)$$

### 9.2.2 Error during a temperature measure within a volume.

In the case of a measure within a volume, we find the three effects seen during the analysis of the measure of a surface temperature. Indeed, according to the thermophysical characteristics, generally different from those of the material, we shall undergo an effect of macroconstriction between the material and the sensor. Furthermore, according to the quality of the setting-up of the sensor within the middle (sensor simply put in contact, sticking or welding), a contact resistance is going to provoke a temperature difference between the material and the sensor. Finally, the third effect seen above is now going to globalize transfers between the material, the sensor and its wires, then between the ambient environment and the wires of the sensor. Really, a difficulty is added here. The fact of realizing a hole with a diameter always higher than the diameter of the sensor under intends to have to analyze transfers between both elements (space between the wires and the hole, contact with grease, glue...).

### 9.2.3 Models of error [3, 4, 5, 6, 7, 8, 9]

We find in the literature a lot of models to describe the errors of measurement by thermocouple. The study of these errors which result from parasite transfers requires the resolution of problems of complex thermal

transfers always varied because of the variety of the configurations and the conditions connected to the environment. It supposes the elaboration of mathematical models adapted to every case.

We suggest first of all presenting a very simplistic but typical model which is going to allow us to highlight the respective roles of the conduction within the middle, of the imperfection of the contact between the thermocouple and the surface, and finally of the exchanges with the environment. This model described in the article of Bardon et al. appears through the three effects seen in paragraph 2.1. Most of the conclusions of this study will then be transposed into various configurations usually met in the practice. We shall successively consider the measures in steady state regime and in transient regime. However, before this, it is necessary to underline that transfers between the wire of the thermocouple and the ambient are defined through a heat transfer coefficient  $h$  and a characteristic temperature  $T_E$  being able to group together the convective and radiative transfers.

$$h = h_r + h_{cv} \tag{9.7}$$

with  $h_r = 4\varepsilon\sigma T_m^3$  and, where  $T_m$  is the temperature between the temperatures of the two surfaces.

**(1) Model in steady state regime for a measure of the surface temperature [3, 7, 8]**

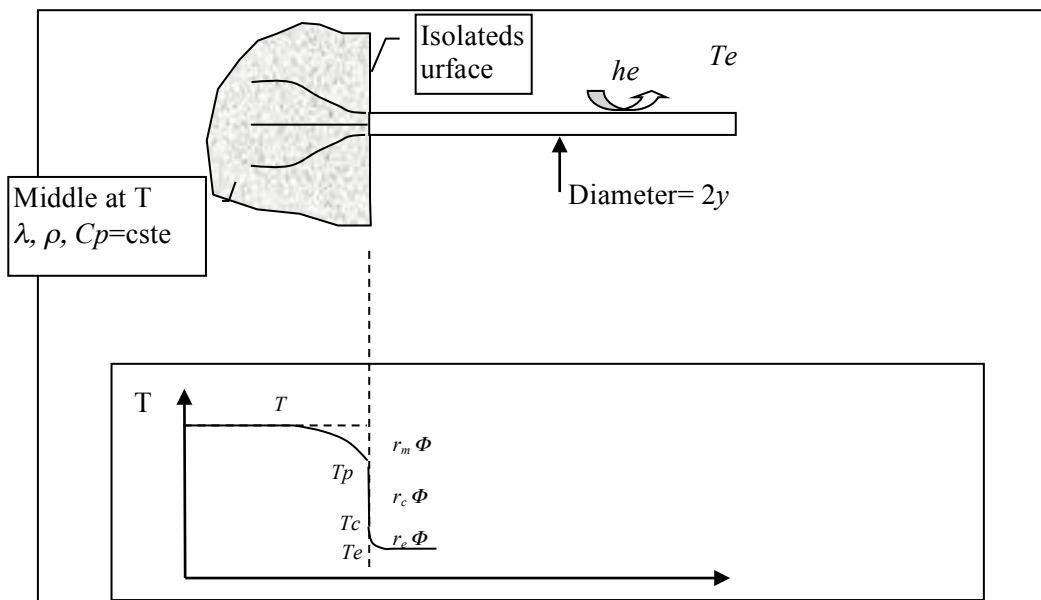


**Figure 3: Model of error in steady state regime**

Let us suppose a measure of temperature on an isothermal surface ( $T$ ) of an opaque semi-infinite middle. For the needs of the theoretical study, we consider only a single wire (measure by semi-intrinsic thermocouple). Figure 3 presents the theoretical scheme. The surface of the middle is supposed isolated. We have only a heat transfer on the contact with the sensor represented by a bar. The modelling of the contact is defined by the three previously seen effects:

- ✓ Effect of the convergence: this effect is defined by a convergence of the heat towards the zone of measure. The temperature  $T$  of the isolated middle is perturbed by the energy pumping in the wire:

$$T - T_p = r_m \Phi \quad (9.8)$$

$r_m$  is the macro-constriction resistance and  $\Phi$  the transferred heat flux. We show with the hypothesis of the semi-infinite middle, the following two expressions:

$$r_m \cong \frac{l}{4y\lambda} \text{ or } r_m \cong \frac{\delta}{3\pi^2 y\lambda} \quad (9.9)$$

As we suppose the circle of contact isothermal or crossed by a uniform heat density ( $\lambda$  is the thermal conductivity of the middle). The calculation also shows that the main part of the temperature disturbance is located in the immediate neighborhood of the circle of contact (94 % of the fall  $T - T_p$  is made inside the sphere of center O and of radius  $10 y$ ).

- ✓ Effect of the contact resistance: responsible for the temperature drop between the perturbed temperature and the measured temperature, it is defined by the relation:

$$T_p - T_c = r_c \Phi \quad (9.10)$$

where  $r_c$  represents the contact resistance for the contact area  $s$  :  $r_c = \frac{R_c}{s}$ . This effect is connected to the imperfection of the contact which results from the roughness of the surface.

- ✓ Effect of fin: it is defined by a heat transfer between the wire and the outside environment. The heat flux is transferred between the face  $x=0$  at the temperature  $T_c$  and the outside environment at an equivalent temperature  $T_e$ :

$$T_c - T_e = r_e \Phi \quad (9.11)$$

where  $r_e$  represents the global thermal resistance of the transfer. It depends on the geometry, on the global heat transfer coefficient  $h_e$  (convection + radiation), and on the conductivity  $\lambda_e$  of the wire. For a bar with a radius  $y$ , the resistance is defined by the relation:

$$r_e = \frac{l}{\pi y \sqrt{2 h_e \lambda_e y}} \quad (9.12)$$

With these three equations, we deduct the error of measure:

$$T - T_c = \delta T = (r_c + r_m) \Phi \quad (9.13)$$

or  $T - T_e = (r_c + r_m + r_e) \Phi$

so

$$\frac{T - T_c}{T - T_e} = \frac{\delta T}{T - T_e} = \frac{(r_c + r_m)}{(r_c + r_m + r_e)} \quad (9.14)$$

$$\delta T = \frac{T - T_e}{\frac{(r_c + r_m + r_e)}{(r_c + r_m)}} \quad (9.15)$$

$$\delta T = \frac{T - T_e}{1 + \frac{r_e}{r_c + r_m}} \quad (9.16)$$

The committed error is thus proportional to the difference between the temperature to be measured and the outside equivalent temperature. The error is all the weaker as the sum of the macroconstriction and contact resistances will be weak when faced with the resistance of outside connection.

We show:

- For measures on a metal with a good conductivity  $r_m \ll r_c$ , it is essentially the contact conditions that set the error.
- For measures on an insulating material  $r_m \gg r_c$ , it is the effect of macroconstriction that sets the error.
- Even in conditions of perfect contact, an error persists depending on the relationship  $\frac{r_m}{r_e}$
- The roles of  $r_e$  and of  $T_e$  are finally very important. It is necessary to have  $r_e$  the biggest possible and  $T_e$  the closest of  $T$ .

These conclusions established in the case of a measure on an opaque middle and for the configuration stylized by a wire having the shape of a perpendicular bar on the surface live for more complex real configurations. In any case, it would now be necessary to study the case of a measure within the middle as well as the cases of the transient regimes.

The objective of this workshop being to be able to take into account measure errors in the inverse analysis, we are now going to attempt to develop numeric models of error to quantify these and define in transient regime the best configurations of thermocouple design.

## 9.3 Application

### 9.3.1 Introduction

Welding is an assembly method in constant evolution. Mainly used by heavy industry, many processes were developed for several years however arc welding is the most harnessed.

Moreover, to ensure joint quality, numerical simulations take on a fundamental importance and try by complementing or making it possible to avoid experimental measurements. Actually, mechanical effects like welding distortions or residual stresses are directly linked to the evolution of the thermal field created by process energy. The difficulties concern, firstly, the simulation of coupled phenomena like the arc and the plasma over the liquid metal, and secondly, the characterization of not well known parameters that are not well known. For these reasons, two levels of simulation can be implemented. The first is named "Multiphysic" and its objective is to model the whole physical phenomena. The second is a simplified thermal simulation with an equivalent heat source.

One way to establish the simplified law of energy distribution is the implementation of an inverse method used in conjunction with thermal measurements. Therefore, the quality of inverse problem results is strongly dependent on the experimental part.

The objective of this work is to investigate the thermal discrepancy between our measured temperatures and temperatures obtained by classical measurements techniques. This study was done to propose an optimal configuration for thermocouple installation. Our study takes place in the determination of an equivalent heat source for M.A.G. process (Metal Active Gas) with filler material and on "T" configuration [10]

### 9.3.2 The goal of the instrumentation

Before introducing bases of instrumentations, an explanation about the different forms of simulation is required. Two classes of numerical models can be distinguished. The first is designed to simulate the process by modelling the whole phenomena. The second is simplified to a pure conduction model, thus, phenomena occurring in the fused zone are neglected or approximated.

It should be noted that much of the studies need a large knowledge of physics parameters like magnetic, hydrodynamic and thermal properties of gas, liquid and solid materials. Moreover, the needed numerical resources are also important and not available in the industrial context. For this reason, simplified models are developed using only the thermal diffusion equation and an equivalent heat source term which represent the effects of phenomena in the fused zone.

#### (1) The equivalent heat source

The “**equivalent source**” simulation is based on the assumption that the real heat distribution is closely approximated by a mathematical function. Therefore, the thermal field is assumed lowly sensitive to the liquid part, or the equivalent heat source must approximate its effects. Mathematical laws complexity is dependent on the approximation level. Indeed, the most simplified expression is the “point heat source” in which all the energy is applied at one surface point. If the real energy input is introduced inside the volume it is possible to simulate it by distributing constant energy along a line. These two kinds of assumptions were mainly used in the past for analytical resolutions. Now numerical simulation and computing evolution allow for the use of more complex laws. When energy has to be applied on the workpiece surface, the Gaussian distribution is the common use. Indeed, it allows for the set-up of the amplitude and the radius. Moreover, for a process which gives energy inside the workpiece volume, the surface equivalent heat source could be used but the theoretical energy had to be distributed along the third dimensions. Several cases can be encountered, energy can stay constant along the depth or it can decrease with a mathematical law, for example, linear or Gaussian.

Nevertheless, the shapes of the approximate heat sources depend on the process which is why several laws are made to be easy to customize. For example, the one which is named: Cylindrical Involution Normal (CIN) is show in equation (15), in a quasisteadystate formulation. The source term is assumed to be constant through time, and after the moving of the space referential on it [11, 12].

$$S(x, y, z) = \frac{kK_z \eta UI}{\pi(1 - \exp(-K_z e_p))} \exp(-k(x^2 + z^2) - K_z y) * [1 - u(y - e_p)] \quad (9.17)$$

Where  $u(\dots)$  is the Heaviside function,  $k$  the concentration factor,  $K_z$  the involution factor and  $e_p$  the depth source application.  $U$ ,  $I$  and  $\eta$  are respectively, the welding voltage (V), current (A) and arc efficiency.  $(x, y, z)$  is a axis system in which  $x$  and  $z$  are tangent and normal to the top surface of filler material.

Others kinds of equivalent heat sources try to include the fluid-mechanic effects. An example of these distributions is the “Goldak's double-ellipsoid” [13], in which the front and the rear ellipsoids (Figure 4) are respectively written with equations (16) and (17).

$$q_f(x, y, z) = \frac{6\sqrt{3}f_f Q}{abc_f \pi \sqrt{\pi}} \exp(-\frac{x^2}{a^2}) \exp(-\frac{y^2}{b^2}) \exp(-\frac{z^2}{c_f^2}) \quad (9.18)$$

$$q_r(x, y, z) = \frac{6\sqrt{3}f_r Q}{abc_r \pi \sqrt{\pi}} \exp(-\frac{x^2}{a^2}) \exp(-\frac{y^2}{b^2}) \exp(-\frac{z^2}{c_r^2}) \quad (9.19)$$

Where  $f_f$  and  $f_r$  are factors of energy deposited on the front and rear parts of  $y$  axis and  $a$ ,  $b$ ,  $c_f$  and  $c_r$  are the Gaussian radius.

The difficulty in these approaches is the determination of these previous parameters because they are not directly related to a physical phenomenon. However, they are estimated by an inverse method, but it compels to perform experimentation. By knowing the real temperatures at a few points and having the numerical simulation at these same points, an identification algorithm compares experimental and numerical temperatures to adjust heat source parameters.

In our study, the equivalent heat source is written with the CIN law and the estimation method is based on the *Levenberg-Marquardt* algorithm. It reduces a quadratic criterion defined as the difference between experimental and numerical temperatures.

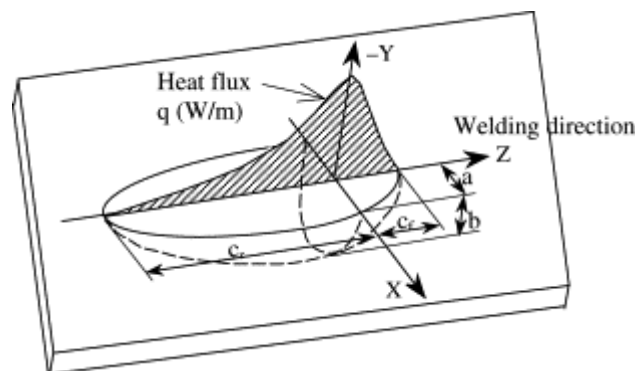


Figure 4: Goldak's double-ellipsoid [13]

Actually, a lot of thermal instrumentations are available to solve inverse problems. Measurements must be performed in a high temperature gradient (sensitivity problem), which means close to the liquid/solid interface. In the next part, some of these methods are explained.

## (2) Welding measurement methods

For the characterization of the heat diffusion in the fused zone, three main measurement methods can be distinguished: observation with high speed cameras, infra-red measurements and thermo-electrical probes.

- High speed cameras are suitable for observations of fluid motion or for measurements of weld pool sizes. However, it gives only surface information. Without temperature measurements this method is impractical for heat source identification but it is possible to use its observations for constrain estimation.
- Thermography and pyrometry are two methods which allow for measurements of infrared radiations. With appropriate relation it leads to surface temperatures. But both are limited by the difficulties to determine the emissivity and they are only able to directly detect surface information. The main advantage of thermography is the high number of sensors (for example: 120\*160) and its ease of implementation. By measuring radiation at two wavelength values, some pyrometers are not subject to emissivity difficulties.
- The use of thermocouple is an intrusive method. The hot junction (Figure 5) has to be in contact with the sample at the exact location where the measurement must be made. So, the way to implement thermocouple inside a solid body is to get it in touch at the bottom of a hole (Figure 5). The drawback is the thermal field disturbance which can occur all around the probe. Furthermore, different "Types" of thermocouples are available, their use depend on temperature levels. In our case, type K thermocouples are used (Figure 5), their maximal thermal charge is 1367°C for 0.15s. Due to this information and because we want measurements that are as sensitive as possible for researched parameters, an implementation plan must be developed.

Figure 5 is a picture showing one of our thermocouples implemented in the sample and presenting the different parts of it. More information is given about this picture in the next sections of this paper. The choice of thermocouple locations is critical for the quality of identification results, the next part explains how we have selected these positions.

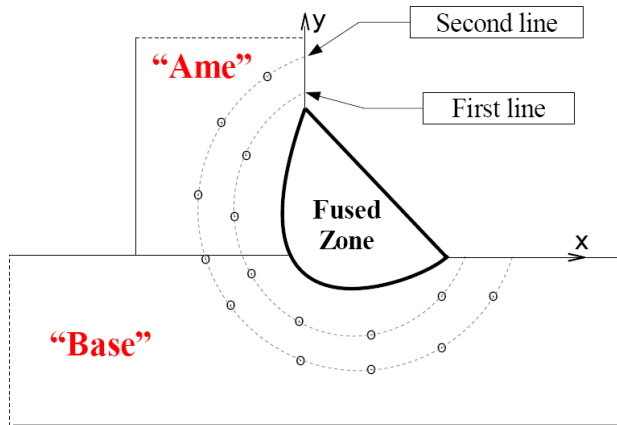


Figure 5: Example of our thermocouple

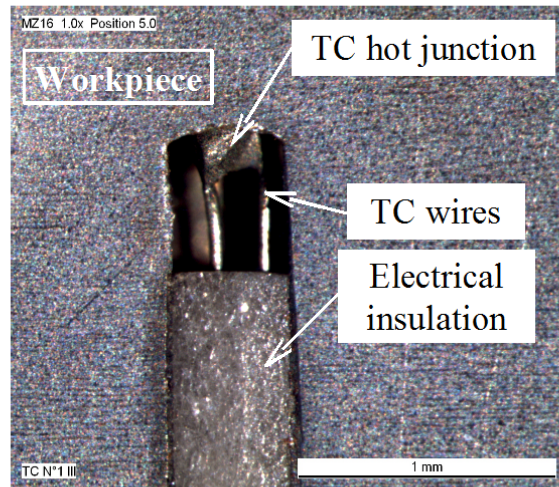


Figure 6: Measurements locations, scheme of macrography

### (3) Thermocouple locations: Thermal gradient measurements

To define a good thermocouple position, several ideas have to be explained. The identification concept is based on observation of the parameter variation effects on the thermal field. This sensitivity decreases when measurements are far off the weld pool. Moreover, a temporal discrepancy is observed. Caused by the thermal capacity of material, those effects can be reduced by introducing thermocouples close to the heat source.

For heat flux identification, one measurement line might permit estimation. Nevertheless, the solution cannot be reliable because several flux shapes can reduce quadratic criterion. For this reason and to stabilize estimation, a second line of thermocouples is realized. So, a three dimensional “picture” of thermal gradient is obtained and stability of the estimation procedure is enhanced.

The goal of the identification is to characterize the gradient versus the three directions of diffusion ( $x$ ,  $y$ ,  $z$ ). So, a finite measurement line is defined around the fused zone limit seen on a scheme of a macrography (Figure 6). According to fused zone uncertainty (caused by weld pool instability) and with a previous theoretical simulation, we define a priori this first line near  $1100^{\circ}\text{C}$ - $1200^{\circ}\text{C}$  (Figure 6). Then, to define correctly thermal gradients, a second line is fixed to observe isothermal lines at  $1000^{\circ}\text{C}$ - $1100^{\circ}\text{C}$ . The third dimension is along the welding direction. We have considered a quasisteadystate analysis; therefore the third dimension is the time multiplying the welding velocity. The  $z$  gradient is, in fact, time variations.

#### 9.3.3 Our welding case

As was previously said, this study takes place in a larger project named: MUSICA [10]. This multi-partner work was initiated by the CEA in collaboration with the French “Welding Institute”, the CETIM, Esi-Group and AREVA. The aim of their work is the development of three software tools designed to allow a non expert user to realize global simulation of welding processes. Indeed, the first is made for the simulation of welding processes, the second for thermo-mechanical simulation at component sides and the third for calculation of distortion effects on multi-component structures. Moreover, those tools coupled to

inverse method and with instrumented equipment permit heat source estimation for usual welding processes like T.I.G. (Tungsten Inert Gas), laser, electron beam welding or M.I.G./M.A.G. (Metal Inert/Active Gas). Those elements need accumulation of knowledge about many welding simulation cases, like ring-shape welding or “T” welding.

This present work deals with the optimal instrumentation for two weld transits and with the heat source identification in the case of “T” welding with filler material.

It should be noted that the industrial aspect of this work has constrained us to not unveil the process parameters or thermal properties of the used material. Each of the given cases will be specified.

### (1) Mathematical model

The best parametric estimation must be performed only with previous experimentations. It allows you to check the “weldability” of the specimen. Two pieces of metal (AISI S355 steel) are used (Figure 7) the “Base” ( $0.5 \times 0.5 \times 0.01 \text{ m}^3$ ) and the “Ame” ( $0.5 \times 0.01 \times 0.1 \text{ m}^3$ ). After the welding test, the sample is cut out, transversal plans are chemically attacked and photographs of weld joints are taken. The main objective of this first experimental part is to create a simplified simulation (Figure 8) which give a fused zone as close as possible to the one observed on previous macrographies. The simulation gives us a thermal field, which is then use to define the location of an a priori instrumentation for the next experimental part designed for the inverse problem.

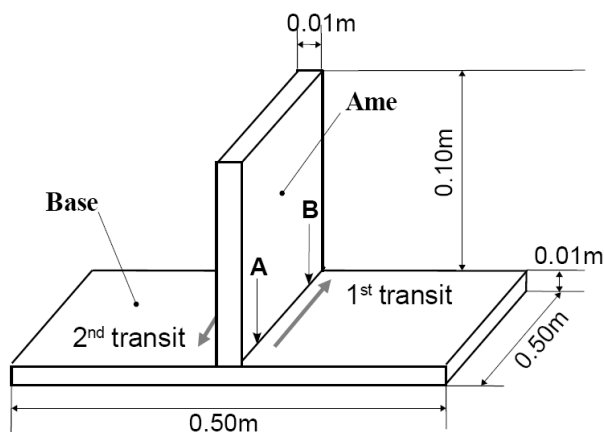


Figure 7: Experimental sample

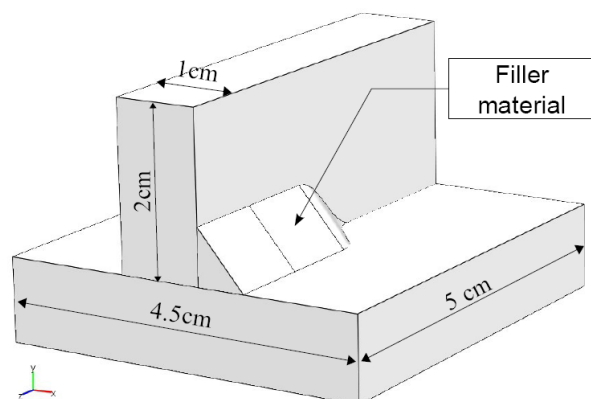


Figure 8: Simulated sample

In Figure 7, we show the two instrumented zones: A for the first transit and B for the second.

The simulated geometry has to be reduced (Figure 8) to decrease calculation time, but dimensions must be sufficient to avoid fused zone disturbances caused by boundary conditions implemented in the model.

The filler material is difficult to simulate, thus we suppose it ever present on the geometry (Figure 8).

A 3D direct problem is solved by the Finite-Element Method with the software Comsol Multiphysic®. This analysis is performed assuming the heat equation in a quasisteadystate conduction according to equation (18). To reduce the degrees of freedom solved, the fluid mechanics and other phenomena are neglected. So, the equivalent heat source  $S(x, y, z)$ , in this heat equation formulation, must represent all

these phenomena in the fused zone and approximate the three dimensional heat distribution. This heat source will be described in the next part. The following equation is the heat diffusion equation:

$$v \cdot \rho(T) \cdot cp(T) \frac{\partial T}{\partial z} = \frac{\partial}{\partial x} \left( \lambda(T) \frac{\partial T}{\partial x} \right) + \frac{\partial}{\partial y} \left( \lambda(T) \frac{\partial T}{\partial y} \right) + \frac{\partial}{\partial z} \left( \lambda(T) \frac{\partial T}{\partial z} \right) + S(x, y, z) \quad (9.20)$$

Where  $v$  is the welding speed ( $\text{m.s}^{-1}$ ) along  $z$  axis,  $\rho$  is the density ( $\text{kg.m}^{-3}$ ),  $cp$  the heat capacity ( $\text{J.kg}^{-1}.\text{K}^{-1}$ ) and  $\lambda$  the thermal conductivity ( $\text{W.m}^{-1}.\text{K}^{-1}$ ).

Thermal properties are isotropic but, for confidentiality reason, they cannot be presented here. Boundary conditions are defined in (Figure 9). In this quasisteadystate simulation, the equivalent heat source is centered on the “S” point (Figure 9) and its “displacement” is simulated (quasisteadystate assumption) along the  $z$  direction. Consequently, a graph showing temperature along the  $z$  axis is equivalent to a thermogram. This is what we need to compare real time measurement with this simulation.

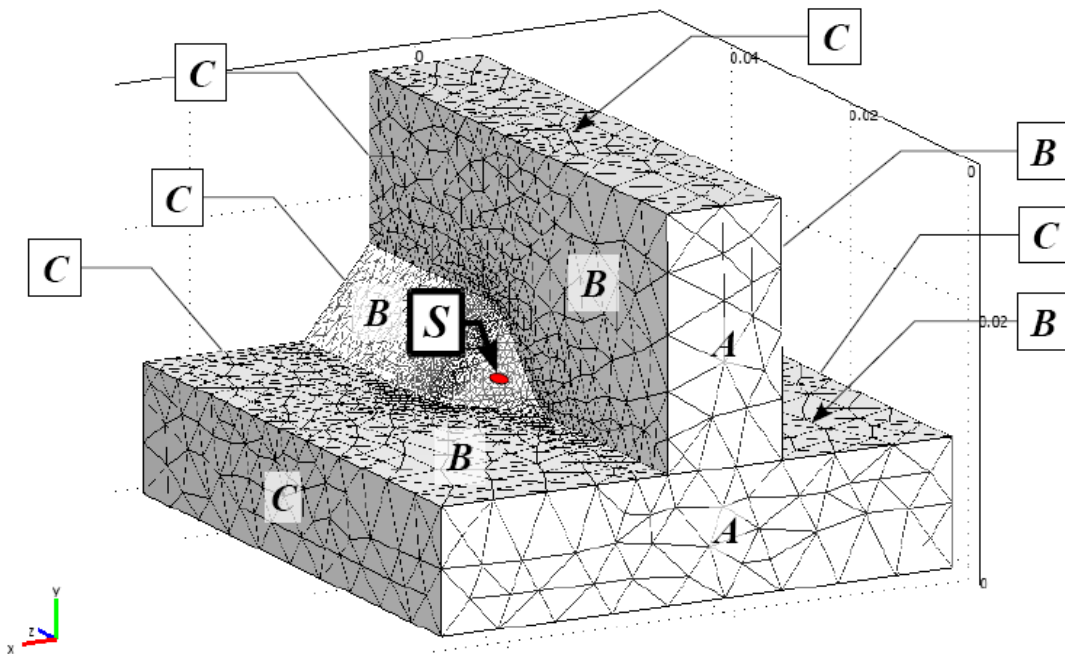


**Figure 9: Mesh and Boundaries conditions**

**(A: Ambient temperature, B: heat losses and C: thermal symmetry)**

- For  $z = 0$ , before the heat source (Figure 9 boundaries A), the temperature is equal to ambient temperature ( $20^\circ\text{C}$ ).

$$T = T_\infty \quad (9.21)$$

- Behind, for  $z = 0.05$  (Figure 9 boundaries C) boundaries are assumed sufficiently far from heat source to be represented by thermal symmetry. The same assumption is realized for boundaries on  $x = -0.02$  and  $x = 0.025$

$$\lambda(T) \frac{\partial T}{\partial n} = 0 \quad (9.22)$$

- Lastly, for boundaries which are in contact with air (Figure 9 boundaries B) we consider that a correct approximation of temperatures is obtained by classical convection and radiation losses.

$$-\lambda(T)\frac{\partial T}{\partial n} = h(T - T_\infty) - \varepsilon\sigma(T^4 - T_\infty^4) \quad (9.23)$$

Where  $h$  is the coefficient of convection ( $\text{W.m}^{-2}.\text{K}^{-1}$ ),  $\varepsilon$  the emissivity and  $\sigma$  the *Stefan–Boltzman* constant.

In the majority of studies, the filler material is ever-present in the workpiece geometry, but elements are activated at the rear of the weld pool which can be approximated with the rear of source application. In our case, the software used do not allow us these kinds of numerical tools, but here, the heat source is stationary and we can directly define the front part of the fused zone geometry. This shape is defined thanks to experimental information and created with a *Bézier's* surface. The latter is built thanks to observations of the filler material after solidification. During the last part of the welding, when the arc disappears, the fused zone is solidified, but the surface shape of the liquid part stays apparent. The mark left by the maximum of the arc pressure could also be located. So, the surface length is twice the distance between the front of the observed weld pool limit and the hole left by the arc. Consequently, by applying the heat source in the middle of the surface, the energy input into the fused zone looks like a good approximation of reality. Indeed, the difficulty is the representation of physical phenomenon which occurs during energy input. The latter is divided into two parts; the first is introduced by the electrical arc (at the surface) and the second by the droplet (in the volume). To simulate these two effects we have located the C.I.N source at halfway of the filler material in the middle of *Bézier's* surface (Figure 9).

## (2) Heat source definition

The aim of this work is the identification of an equivalent heat source law. The mathematical expression of  $S(x,y,z)$  is assumed to be a Cylindrical Involution Normal (C.I.N) as defined in equation (15) but with modified axis, as (22):

$$S(x,y,z) = \frac{kK_z \eta UI}{\pi(1 - \exp(-K_z e_p))} \exp(-k(v^2 + z^2) - K_z w) * [1 - u(w - e_p)] \quad (9.24)$$

$(v, w, z)$  is a modified axis system in which  $v$  and  $w$  are tangent and normal to the top surface of filler material. The main advantage of this voluminous heat source is the small number of unknown parameters:  $k$ ,  $K_z$ , and  $e_p$  the depth source application.

The inverse problem has to find values of CIN parameters; however, the validity of this energy input shape must be checked. The direct problem is solved using different source parameter configurations. Several melted zones are shown in Figure 10.

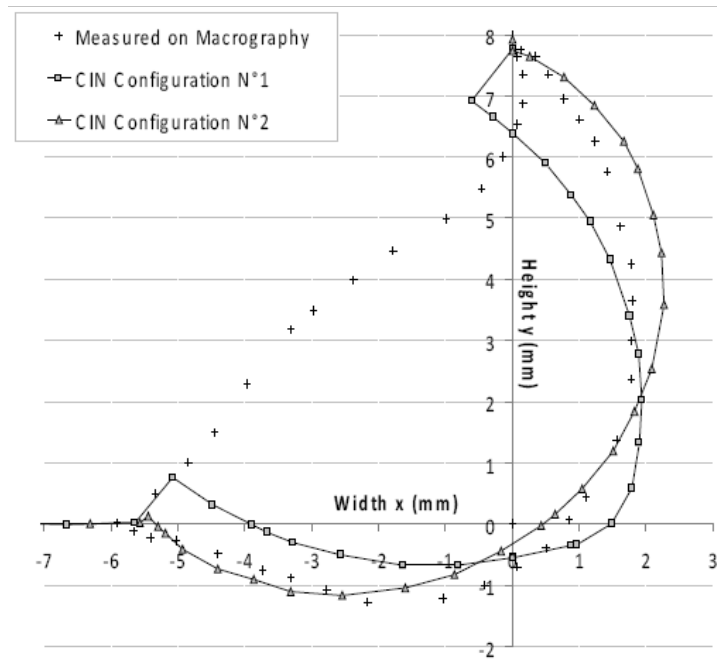


**Figure 10: Melted zones for two sources**

The choice of heat source parameters is not easy, but as showed in the Figure 10, weld pool observed on a macrography can be surrounded by the results of two parameter configurations. The “*CIN configuration N°2*” has the good width but the depth is too low, inversely, the “*CIN configuration N°1*” has an insufficient width but the depth is too great. This means that the mathematical law is able to simulate energy input which validates the shape of the melted zone, but the use of the inverse method is necessary to avoid the manual parameterization. Moreover, macrography allows only for a partial validation (plan  $Oxy$ ) of the fused zone limit. Indeed, the shape along the  $z$  axis (or time evolution) cannot be checked this way. So, the good heat source term will be found only after resolution of the inverse problem because estimation is realized with temperature measurements throughout time, which is the third dimension of our quasisteadystate model.

Model used to obtain Figure 10 results is defined with tetrahedral mesh elements. The software Comsol Multiphysics is already fitted with an automatic mesh creator which allows the definition of the maximal sizes of boundary or volume elements. The numerical sample is too big for a global definition of a thin mesh, but for our case the interesting zone is near the weld pool. So, only elements on volumes of filler material are refined at 0.0015mm of maximal size. Other volumes are freely meshed, but with a growing factor equal to 1.1. The number of elements is close 40000 elements. The validation of this mesh is realized by comparing these results to others obtained with the same simulation but discretized more thinly (higher than 60000 elements). By observing the shape of the phase change temperature, which is very close in both cases, it is possible to conclude that the first mesh is sufficiently thin.

### **(3) Inverse problem method and experimentation plan**

In this study, the inverse problem reduces a quadratic error built on the difference between temperatures which results from the direct problem and experimental measurements, such as equation (23). The used method is the Levenberg-Marquardt algorithm which calculates new parameters with the iterative expression (24). It is an association of the steepest and Gauss-Newton methods, which allow for an important estimation speed and a good hardness.

$$S(n) = \sum_i (Y(i) - M(i))^2 \quad (9.25)$$

$$p^{n+1} = p^n + [J^T J + \lambda^n \Omega]^{-1} J^T (Y - M(p^n)) \quad (9.26)$$

With:

$$J = \frac{M(p^n + \varepsilon p^n) - M(p^n - \varepsilon p^n)}{2\varepsilon_v p^n} \quad (9.27)$$

Where  $n$  is the iteration step and  $P$  is the estimated parameter.  $J$  is the sensitivity, in our case; it is obtained by the numerical derivation of modeled temperature over parameter variation (25).  $Y$  and  $M$  are respectively measured and simulated temperatures.  $\lambda$  is a damping factor and  $\Omega$  a diagonal matrix defined to offset measurement noises. The  $\varepsilon_v$  factor is the variation step of parameters.

In equation (25), it is possible to observe the link between thermal measurements and parameter estimation. As a consequence, the estimation of the heat source needs a very accurate experimental investigation. Situation and number of temperature measurements have an impact on the parameter quality.

To ensure efficient parameter identification, thermocouple positioning must respect four principles related to the measurement theory and previous observations [3]:

- The thermal field is a picture of energy distribution. Measurements have to be given all around the melted zone.
- For sensitivity reasons, the thermocouple must be as close as possible to the weld pool.
- The thermal gradient measurement in three dimensions can be useful.
- Information observed throughout time gives the third dimension gradient (quasisteadystate assumption).

With the previous advice, we define an a priori location of thermocouples as show in Figure 11. The validation of this plan is realized by a theoretical inverse problem.

### 9.3.4 Theoretical inverse problem

#### (1) Estimation without measurement noise

Before parametric identification with experimental temperatures, it is necessary to check, theoretically, several points like which parameters it is possible to estimate with the previous implementation plan.

For this reason, a sensitivity analysis is made. Two elements are important, amplitudes of sensitivities and linear dependences of parameters. In the first case, no sufficient amplitude signifies that a parameter variation involves too low of a difference on the thermal field, its effect is the difficulty, and the increase of the time to estimate. In the second case, if two parameters are linearly dependent, a variation of each of them produces the same effects on the thermal field. Therefore, a small change of the first parameter can balance the one of the second and the algorithm is not able to estimate parameters.

The previous theoretical model is used as a direct problem and as a “numerical experimentation” with reference parameters. The latter are defined to have a melted zone quite close to the one observed on macrographies.

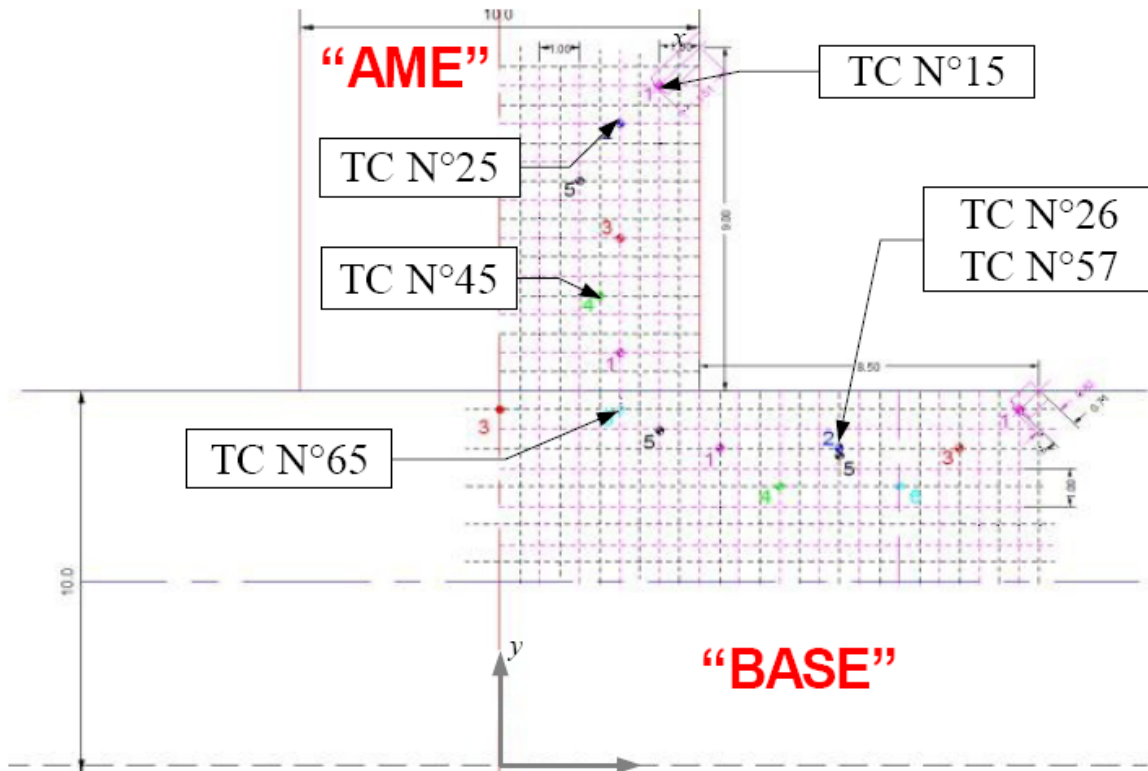


Figure 11: Theoretical location of thermal measurement

The parameter choices are realized after manual “*identification*”, so the melted zone shape is not perfect with regards to macrographies, but sufficient to perform this analysis. We have kept:  $k=57000\text{m}^{-2}$ ,  $K_z=370\text{m}^{-1}$  and  $e_p=0.012\text{m}$ .

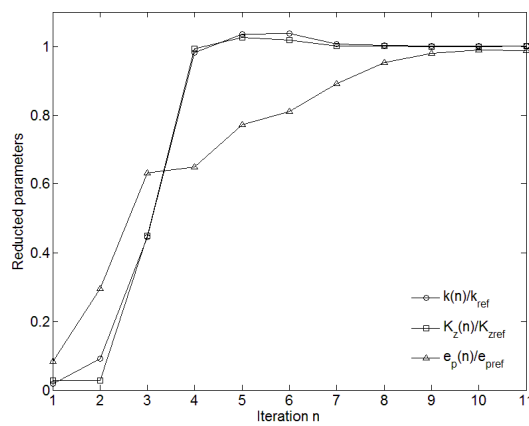
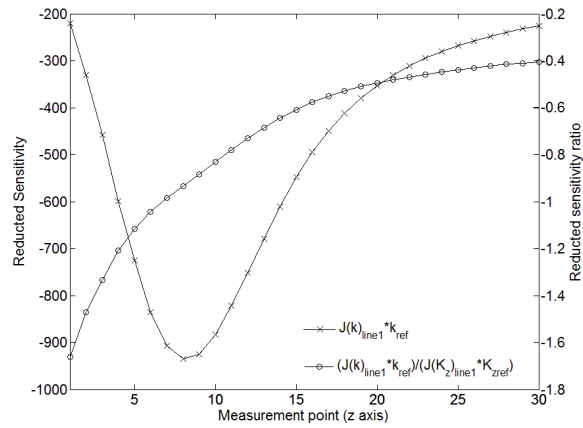
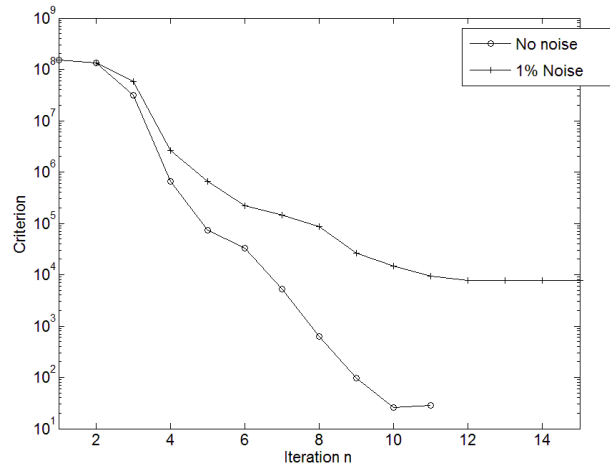


Figure 12: Check of sensitivity amplitudes and linear dependences



**Figure 13: Parameters evolution**

With this heat source, the first analysis concerns sensitivity coefficients presented by equation (25). In Figure 12 it is possible to observe the sensitivity of the first parameter ( $k$ ) on the first measurement line at  $x=0.004m, y=0.018m$  and along  $z$  axis. It should be noted that the real sensitivity amplitude is obtained by multiplying coefficients by the reference parameter. Obviously this kind of curve must be realized for each parameter and at each measurement coordinate but we cannot show them in this paper. Observations are related with theoretical thermocouple locations. First thing, the  $k$  parameter, which is the concentration factor, has more influence over the thermal field near the surface. Consequently, sensitive thermocouples are these which are close to the surface, like TC N°15 in the Figure 11, and amplitudes of variations observed are sufficient for estimation (approximately  $900^{\circ}C$ ). Second thing, the  $K_z$  parameter is the involution factor and it affects the middle part of the heat source by making it more cylindrical or more conical. So, in this case, sensitive thermocouples are these located by the sides of the fused zone, TC N°45 in the Figure 11. And third thing, the depth penetration  $e_p$  of heat source produce variation underneath the simulated weld pool, and measurements are sensitive near the lower extremity of heat source, TC N°65.



**Figure 14: Criterion reduction during identification**

The second curve in Figure 12 is the ratio between two parameter sensitivities. Here, it is the case of  $k$  sensitivity divided by the one of  $K_z$  and this also along the first measurement line. This ration had to be made for all parameters and for all measurement coordinates. Their aim is the search for linear dependences (previously explained). If this ratio is equal to a constant value, parameters are linked and the estimation will fail. In Figure 12,  $k$  and  $K_z$  are clearly independent on this “thermocouple”. Conclusions are the same for other parameters, only several measurements are partially dependent but this is caused by their low sensitivities.

This validation is implemented with theoretical thermocouple locations chosen for the first transit (Figure 11). A satisfactory estimation is obtained after ten iterations with a final criterion equal to 27, which signify a mean error of 0.24°C. The decrease of the latter can be observed in Figure 13.

Figure 13 shows evolutions of parameters dividing referential parameters, this, to observe variations in the interval [0;1] and to be able to compare them. The first two parameters  $k$  and  $K_z$  have equivalent progress. Their final values, respectively 57032 m<sup>-2</sup> and 370 m<sup>-1</sup> are very close to references and convergences are obtained quite quickly. The thirist parameter is  $e_p$ , its identification take more time than previous parameters and the final value is not perfect, near 0.01185m but tends to evolve in the good way.

## (2) Estimation with simulated measurement noise

The interest of this theoretical method is to test the estimation algorithm. Indeed, the previous test is done with “*numerical measurements*” which are not realistic but allow for sensitivity analysis. Nevertheless, before the estimation with experimental temperatures, we have to check if the measurement noise will cause failure of estimation.

For this, inverse and direct problems are the same as before, but an artificial noise is created with a random function. The level of this perturbation is chosen as close as possible to the real measurement noise, which signifies nearly 1% of the maximal signal or 15°C. In this case we only present the criterion decrease. As show in Figure 13, the noise induces estimation after more iteration than before: 15 iterations. Moreover, the criterion is stabilized at a higher value (3800) which is equivalent to a mean error of 5°C in each measurement. Parameters are quite correctly estimated and final values are 56980m<sup>-2</sup>, 370m<sup>-1</sup> and 0.0121m respectively for  $k$ ,  $K_z$  and  $e_p$ . These values are very satisfactory, and with these data; we can assume that the experimental inverse problem will be a success.

Results are summarized in the table 1.

**Table 1: Results of the estimations**

	$k$	$K_z$	$e_p$	Criterion
Reference	57000	370	0.012	
Without Noise	57032	370	0.01185	27 (~0.25°C)
With 1% Noise	56980	370	0.0121	3800 (~5°C)

## 9.3.5 Experimental design

### (1) Experimental implementation

In our study, we use 32 thermocouples introduced inside the workpiece through the Base. This choice of implementation is imposed by the industrial term of reference, for example, we can only drill the workpiece from its back side. We use Type K thermocouples to observe large amplitudes of measurement. TC wires are 50µm diameter and the hot junction is 220µm diameter. To observe workpiece temperature

the contact between the thermocouple and workpiece had to be perfect, so TCs are welded (Figure 5) to sample by capacitive discharge.

To follow ideas proposed in paragraphs “**Welding measurement methods**” and “**Thermocouple locations: thermal gradient measurements**”, measurements are realized along the 1100°C isotherm, nearly 1mm after the melted pool limit (Figure 11). The location of this isothermal line is realized with a previous experimentation without instrumentation in association with a simplified model. The simulation parameters are approximately chosen to obtain a melted zone close to the one observed on the first macrography. Finally, the simulation gives us the shape of isothermal lines. This instrumentation method assumes the repeatability of the welding procedure process, which means that two welding procedures with the same process parameters (current, tension ...) produce a melted zone with the same dimensions. The high number of thermocouples (15) forces us to divide them into six plans orthogonal to the weld direction and spaced by 4mm as show in Figure 15.

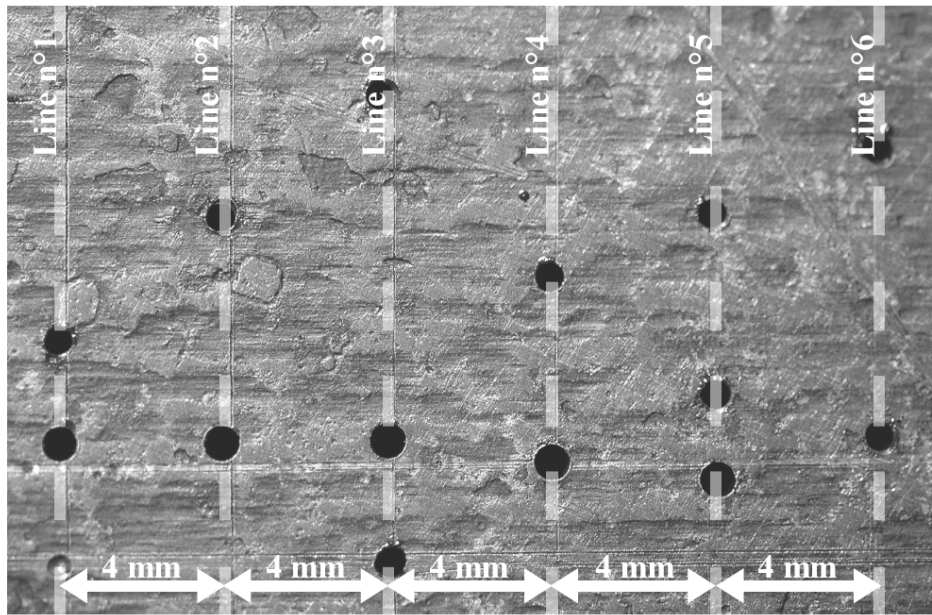


**Figure 15: Hole locations on the back side of the sample “Base”**

Experimentations have been realized by the French Welding Institute in Yutz, the 11th of April 2008.

## **(2) Measurements results**

Results of the inverse problem are directly dependent on thermal measurements, for this reason experimental temperatures are firstly analyzed and after, the link with estimation difficulties will be established.

For the first transit, all thermocouple outputs are in Figure 16 and Figure 17. In the first one, it is possible to observe the failure of TC N°36 located at  $x = 3 \text{ mm}$  and  $y = 14 \text{ mm}$  (cf. Figure 11 for axis origin). The flat signal shows that the problem is not inherent in the welding conditions.

It should be remarked that the time-lag of each curve is a consequence of the space dispersion of thermocouples (Figure 15).

On previous curves another singularity is observed. Two thermocouples, whose coordinates are theoretically same ( $x = 8,5 \text{ mm}$  and  $y = 8.5 \text{ mm}$ ), have very different maximal temperatures. The discrepancy between TC N°26 in Figure 14 and TC N°57 in Figure 17 is nearly 300°C. The first reason which can explain this error is drilling accuracy. Holes, where thermocouple hot junctions are welded, can be realized with low depth differences and the very high thermal gradient induces this error. The second

reason is link to the filler material; indeed, droplet configuration is globular and induces variations in melted pool limits along the weld direction. As previously stated, measurements are implemented into six plans spaced by 4mm. Consequently, thermal field differences appear between plan number 2 and plan number 5.

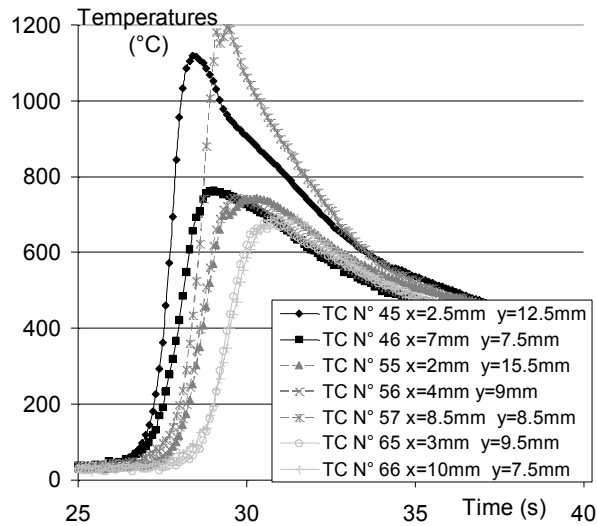


Figure 16: Thermocouples measurements on three lasts' plans

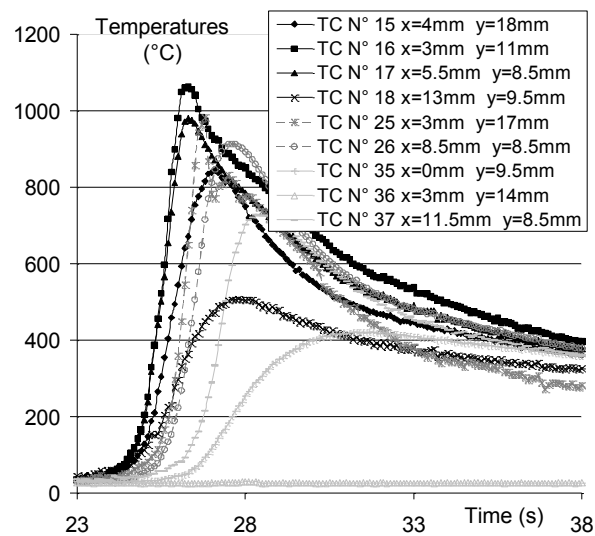


Figure 17: Measurements on three firsts' plans

These explanations are also valid for other cases, for example, TC N°16 in Figure 16 and TC N°45 in Figure 17, which are equidistant from the melted pool limit. They observe different temperature amplitudes and have different evolutions throughout time. It should be noted that holes are respectively parallel and perpendicular to isothermal surfaces. Moreover, the temperature of perpendicular thermocouple increases more quickly and maximal thermal level is higher than the one of the parallel thermocouple. Nevertheless, the cooling of both is quite equivalent which leads one to suppose another

cause. In fact, when the thermocouple hole is perpendicular to isothermal lines this means it is along the thermal flow direction and thus, it block thermal diffusion in this direction which induces thermal accumulation on the hole head [14]. Conversely, when the hole is parallel to isothermal surfaces, it is perpendicular to the flow and heat diffusion is less disturbed. Considering this effect, it is possible to understand previous differences, accumulation makes observed temperatures higher and more quickly but there is no effect during the cooling when the flow is reduced.

To check drill accuracy, real positions of hole heads are observed. For this, workpiece is cut along each measurement plan, polished and chemically attacked. With these macrographies and knowing the thickness of the Base and the “Ame”, it is possible to adjust positions of measurements. For example, the two previous thermocouples with same theoretical coordinates are in reality at: TC N°26  $x = 8.2 \text{ mm}$   $y = 8.4 \text{ mm}$  and TC N°57  $x = 7.8 \text{ mm}$   $y = 8.4 \text{ mm}$ . Thus, in reality the first thermocouple is less close to the melt zone than the second that explains the thermal difference.

Another phenomenon occurs during the welding and has probably disturbed the thermal measurement. It is the displacement of the vertical part over the horizontal part of the workpiece. Despite previous static spots made to seal samples together, the gap hassled by the first transit is  $300\mu\text{m}$  which is nearly half of a hole diameter. Considering this displacement implies the use of thermo-mechanical simulation and it becomes a more complex problem. We assume that the thermocouple has moved with the vertical part, and thus relative distances between the melted pool and the thermocouples are constant and can be neglected.

In an inverse problem, it is important to compare equivalent measured and simulated information, which is why simulated temperatures are extracted from the model at the real coordinates.

### (3) Inverse problem results

The Levenberg-Marquardt algorithm has been implemented with the software Matlab and the direct problem (the model) is run on Comsol Multiphysic which uses the finite element method. It should be noted that estimated parameters are: the concentration factor  $k$ , the involution factor  $K_z$  and the depth of source application  $e_p$ . Other process parameters, like weld current and voltage, are known because they measured during the welding. For confidential reasons we cannot quote them in this paper, however, it should be interesting to note the acquisition parameters like the step time  $0.1\text{s}$ , the total acquisition time  $240\text{s}$  and the weld speed  $5\text{mm}\cdot\text{s}^{-1}$ . Those values are used to convert the time on thirst space dimension implemented on the simulation thanks to the quasisteadystate assumption. Moreover, before estimation, the time-lag observed in Figure 16 and Figure 17 had to be corrected thanks to the weld velocity and the instrumentation line spacing.

Measurements are realized all along the weld period, it is thus necessary to choose the best interval which allows for an efficient estimation. This time duration is chosen according to sensitivity coefficients.

In Figure 18, the sensitivity of the concentration factor along two measurement lines, the first is TC N°15 located on  $x = 4\text{mm}$  and  $y = 0.018\text{mm}$ , the second is TC N°65 on  $x = 0.003\text{mm}$  and  $y = 9.5\text{mm}$ .

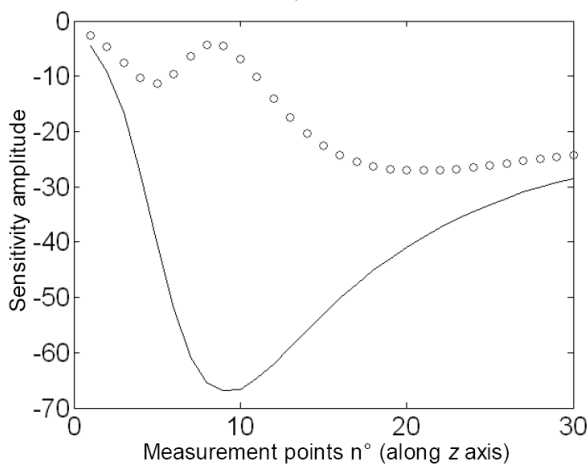


Figure 18: Sensitivity of concentration factor along two thermocouples (dots = TC N 65, line = TC N 15)

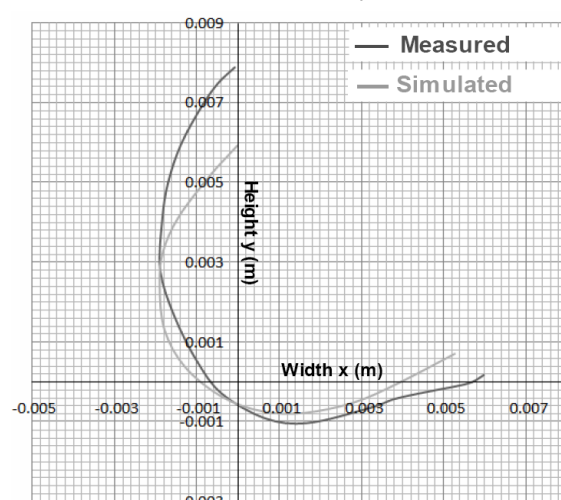


Figure 19: Measured and estimated melted zone limits

The concentration factor is a parameter which indicates the width of the heat source (1) and (8) and the two thermocouples: TC N°15 and TC N°65 are respectively near and beneath the melted zone. As previously stated, the melted pool shape is directly linked to heat source law, and variation effects of the concentration factor can be seen near the workpiece surface (Figure 18). For that reason, sensitivity is more important on TC N°15 than on TC N°65. The same observation could be realized for the involution factor which also defines the shape of the heat source. Indeed, TC N°65 is more sensitive to depth variations and the TC N°15 does not observe any width variation. Figure 18 abscissa is the number of measurement points used for identification, the step time is 0.2s with a weld speed of  $5\text{mm}\cdot\text{s}^{-1}$ , thus the space measurement step used in estimation is 1mm.

The selection of time (or thirist space dimension in the model) interval is realized using curves like Figure 16, the measurements kept are those which have maximal sensitivities and which do not create linear dependences. When measurements are too far from the heat source, all sensitivities are very close to zero and linear dependences appear in each case, as a consequence, it is necessary to keep only the more sensitive measurement points. We have used 15 measurement lines with 30 points per line, which means 450 comparison points.

Results of identification are not satisfactory; the end criterion value is very high. Moreover, the melted zone limit obtained with estimated parameters does not correspond to those observed on macrographies (Figure 19). Differences between the two shapes of weld pool are by a majority located on the surface where the heat source is defined by concentration factor. In the depth of the material the two shapes are close enough; the algorithm does not seem able to enlarge the surface part without increasing depth penetration. This fact leads to reviewing measured temperatures, which gives improper information and to reassessing effects of thermal accumulation previously cited.

To study thermal disturbances caused by thermocouples, we have to develop a new analysis. Thermocouples were included in simulation, thus we will be able to calculate the level of discrepancies.

#### (4) Thermocouples simulations

This work has two objectives, the first concerns quantification of thermal disturbances caused by instrumentation in implementation configuration. Indeed, the theory of thermocouple measurement recommends that holes are drilled parallel to the isothermal surfaces, but in our case the industrial requirements impose a perpendicular direction.

The second is the comparison between different kinds of thermocouples and the determination of effects caused by their implementation. New simulation needs a new definition of the mathematical problem which is firstly presented, then the two kinds of thermocouples are described and lastly, they are numerically implemented in several configurations.

#### (5) New mathematical model

In the present work thermocouples are simulated with workpiece geometry, as a consequence the previous assumption concerning quasisteadystate is no longer usable. Indeed, quasisteadystate is obtained when the thermal field is, in each step time, the same for a referential located on heat source axis, which is not realistic when the thermocouple is in the workpiece.

Thus, the solved equation stills the heat conduction but now in transient analysis (26).

$$\rho(T).cp(T)\frac{\partial T}{\partial t} = \frac{\partial}{\partial x}\left(\lambda(T)\frac{\partial T}{\partial x}\right) + \frac{\partial}{\partial y}\left(\lambda(T)\frac{\partial T}{\partial y}\right) + \frac{\partial}{\partial z}\left(\lambda(T)\frac{\partial T}{\partial z}\right) + S(x,y,z,t) \quad (9.28)$$

It is interesting to note that the heat source term is presently a time function and defined in equation (27).

$$S(x,y,z) = \frac{kK_z\eta UI}{\pi(1 - \exp(-K_z e_p))} \exp(-k(v^2 + (z - vt)^2) - K_z w) * [1 - u(w - e_p)] \quad (9.29)$$

This expression allows a heat flow shape like previously but it travels across the workpiece along the  $z$  axis. Parameters  $k$ ,  $K_z$  and  $e_p$  are not a well-known cause of the failure of the inverse problem. As a consequence, tests have to be realized to set them at coherent values.

Only one boundary condition is modified, it is the one which is named A in Figure 9. The new expression is like other “cut” surfaces, which signify, like equation (20). These adiabatic conditions (Figure 20) are also no longer valid because now, the heat source is not sufficiently far from them, at “the beginning” and at “the end”. However they are kept because thermocouple temperatures are not disturbed by them. On all thermocouple boundaries, convective and radiative heat losses are assumed and defined as equation (21). Other simulation parameters are kept, only thermocouple geometry has been introduced into the workpiece and will be explained in the next part.

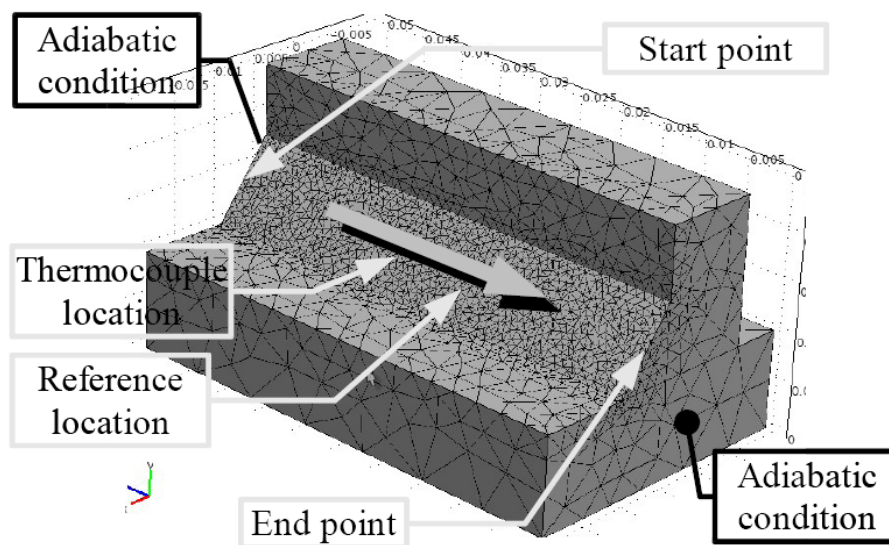


**Figure 20: New boundary conditions and heat source run**

As shown in Figure 20 the filler material is now ever-present all along the workpiece. The longitudinal shape of the fused zone is thus different than the real case. But, for this analysis we do not try to simulate the perfect weld pool shape and an approximation with coherent thermal levels is sufficient.

### **(6) Thermocouple simulations**

The origin of this study is the collaboration with the industrial company. As the time needed to implement laboratory instrumentation is very important, it could be interesting to observe effects caused, on the thermal field, by the use of industrial thermocouples. An experimental investigation could be realized but, as we have previously said, it is very difficult to install two thermocouples at the same coordinates. Therefore, this analysis is performed using numerical simulations.

Laboratory thermocouples are those described in “**Instrumentation implementation**”. Made by ourselves, thermocouples are only composed of the hot junction and the two wires. Materials used are Nickel Chromium - Nickel Alloy (Type K), mean thermal properties of which are noted in the Table 2. The hot junction is assumed to be an ellipsoid with  $320\mu\text{m}$  for high diameter and  $240\mu\text{m}$  for short diameter, wires are  $54\mu\text{m}$  diameter and the hole is  $650\mu\text{m}$  diameter (Figure 21-1).

The industrial thermocouple is also constituted of hot junction and wires but it is sheathed with stainless steel AISI 304L (Figure 21-2). The sheath is  $250\mu\text{m}$  diameter, the hot junction is a  $240\mu\text{m}$  diameter sphere

and wire holes are the same as before. The selection of this thermocouple is made to have an equivalent geometry to a laboratory thermocouple.

Geometry characteristics of laboratory thermocouples are observed on macrographies (Figure 21-3) and some features, such as size of contact surface, are measured on pictures realized by Scanning Electron Microscope (SEM). Industrial thermocouple geometry is created using some information found in manufacturer documentation: *Thermocoax*.

**Table 2 : Thermal properties**

Material	$\lambda$ (W.m <sup>-1</sup> .K <sup>-1</sup> )	Cp (J.kg <sup>-1</sup> .K <sup>-1</sup> )	$\rho$ (kg.m <sup>-3</sup> )
TC	25	445	8600
Sheath (AISI 304L)	15	470	7800

The numerical design of thermal contact between laboratory thermocouples and the workpiece is assume to be perfect (welded). In the industrial case, the thermocouple is assumed to be put down to the bottom of the hole. This implementation is much faster than the laboratory case but induces bad contact quality. This quality is assumed to be symbolized by thermal contact resistance  $R_c$ .

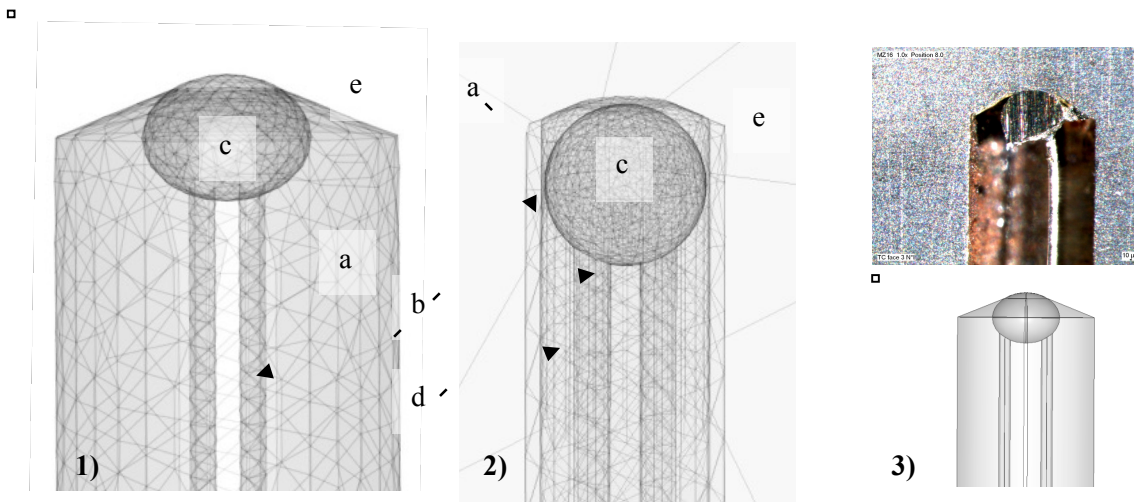


**Figure 21: Geometries for 1) laboratory thermocouple, 2) industrial thermocouple and 3) comparison between simulation and macrography.**

**(a is hole, b are wires, c are hot junctions, d the sheath material and e the workpiece)**

It should be noted that the numerical implementation of thermocouples induce an important increase in the number of freedom degrees we have to solve, thus, it is impossible to simulate all of them at once. Moreover, it seems to be obvious that thermal disturbance will increase with thermal gradient, therefore, only TC N°45 (Figure 10), located on  $x = 2.5\text{mm}$  and  $y = 12.5\text{mm}$ , is examined. Relevance of the latter are its high temperature level (near 1100°C) and its implementation ease for each configuration.

## (7) Numerical tests and results

An objective of this work is the understanding of inverse problem failure and the observation of effects caused by instrumentation quality. As a consequence, the first test deals with implementation orientation, and the second compares results of the industrial and laboratory thermocouples.

As said in the previous part, the TC N°45 is interesting because its location allows for different directions of the implementation. Moreover, it is the one which poses problem in the “**Thermal measurements results**” part. The maximal temperature observed by this TC seems to be overestimated regarding an equivalent measurement implemented parallel to isothermal surfaces. The method to confirm this point is to simulate two cases. One with real thermocouple implementation which means perpendicular to isothermal surfaces and another at the same coordinates but implemented parallel to isothermal surfaces.

For the second analysis, thermocouple evacuation is fixed along the heat flow, which corresponds to the previous second simulation. The bottom of the hole is also positioned at the same coordinates and the contact area is assumed to be maximal what is represent all sheath diameters. In this case, four values of thermal contact resistances are set:  $RC1 = 1.10^{-4} \text{ K.m}^2.\text{W}^{-1}$ ,  $RC2 = 1.10^{-5} \text{ K.m}^2.\text{W}^{-1}$ ,  $RC3 = 1.10^{-6} \text{ K.m}^2.\text{W}^{-1}$  and  $RC4 = 1.10^{-7} \text{ K.m}^2.\text{W}^{-1}$ , where the first is a bad contact and the last is a good contact.

Results in Figure 22 are temperatures observed in hot junction between the two thermocouple wires. To have a referential, temperatures are read at the same x and y coordinates but after thermocouples where there is no longer accumulation.

Concerning the first analysis, observation of discrepancy caused by thermocouple implementation, Figure 22 clearly shows thermal accumulation on the thermocouple head. The perpendicular TC start to overestimate temperatures near  $t = 5\text{s}$  and give again good values near  $t = 8\text{s}$ , whereas parallel TC observations are merged with referential during the entire time. This time interval corresponds with the one which is selected for the inverse problem, in other words, when sensitivity coefficients are maximal. Nevertheless, the time delay induced by the diffusion inside the parallel thermocouple induces discrepancy (Figure 23) but the time in which it occurs is outside the one used for estimation.

In the experimental case, not all thermocouples are along heat flow, therefore, some temperatures are overestimated and others not. These observations explain why estimation has failed. In fact, algorithms try to reduce the criterion defined as the difference between measured and estimated temperatures by varying parameters. But when temperatures are disturbed and not disturbed, parameters are different which lead to previous criterion stagnation with false heat source law.

The second analysis gives information concerning effects of measurement context, industrial or laboratory, and also with regards to implementation quality. In a first time, the worst contact, when  $RC = 1.10^{-4} \text{ K.m}^2.\text{W}^{-1}$ , induces an important a misjudgment of temperatures. The measurement discrepancy of the maximal temperature is higher than  $300^\circ\text{C}$  and with nearly 1.1s delay. These two values lead to understand temperature discrepancies in “Thermal measurements results”, when two measurements at the same coordinates have gave different thermal evolutions. The time delay (Figures 16 and 17) between maximal temperature of TC N°26 and TC N°57 is round about 3.6s, in which a part results from plan spacing. There is 12mm between plan n°2 and n°5 (Figure 15), the speed is  $5\text{mm.s}^{-1}$  thus delay should be 2.4s, but it remains 1.2s. Thus it is possible to conclude that contact quality of TC N°26 is not perfect. Moreover, its heating and cooling rate are too low according to TC N°25 which is closer to the melted zone (observed on macrographies), this can be explained by diffusion difficulties to go through contact resistance. The curve with  $RC = 1.10^{-5} \text{ K.m}^2.\text{W}^{-1}$  shows the same results concerning maximal value and time delay but with less perturbation. When  $RC = 1.10^{-6} \text{ K.m}^2.\text{W}^{-1}$  and  $RC = 1.10^{-7} \text{ K.m}^2.\text{W}^{-1}$  the effects of contact resistance is negligible and information is close to reference. Industrial thermocouples are thus able to measure true temperatures but the contact quality must be very good by using, for example, heat-sink grease.

The industrial thermocouple is perpendicular to isothermal surfaces but the ones with best contact do not have overestimated temperatures. Indeed, the important diameter of sheath material (304L) allows for heat evacuation along the thermocouple and helps avoid heat accumulation.

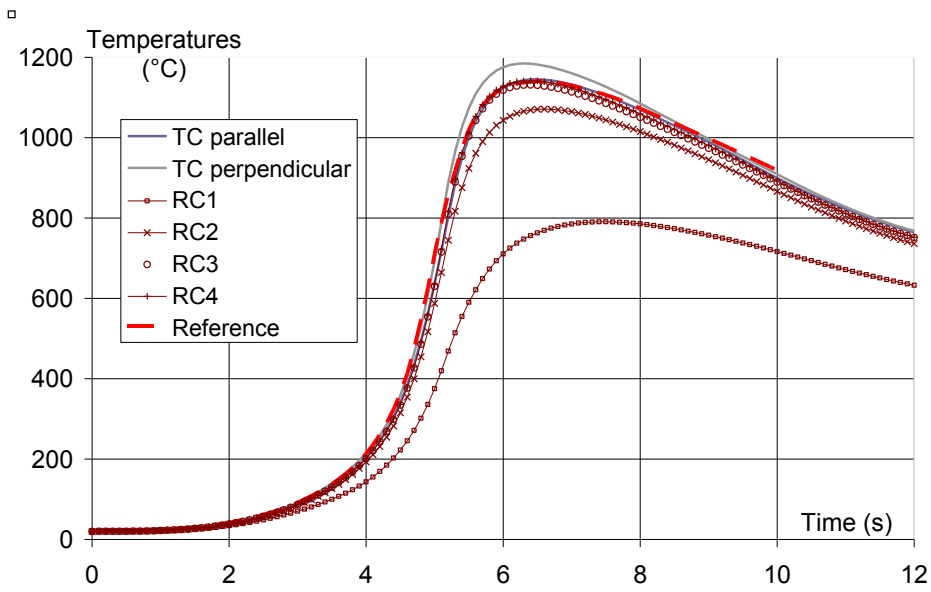


Figure 22: Thermal measurements

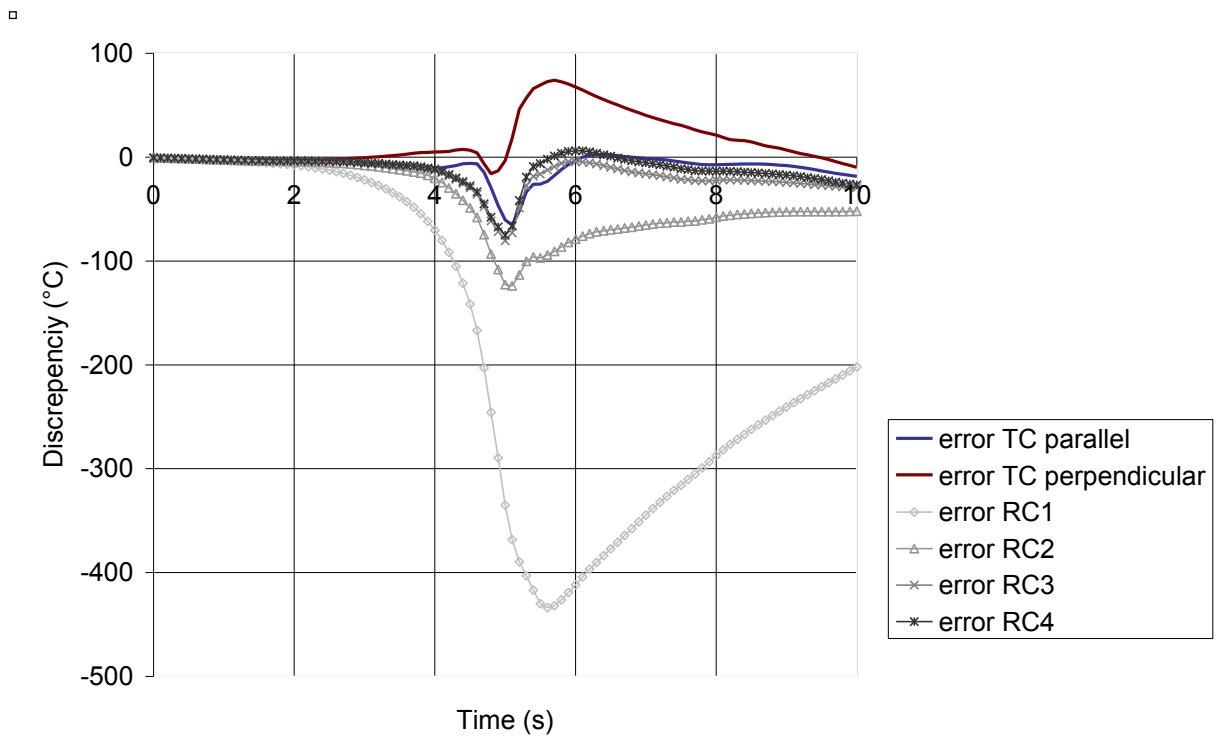


Figure 23: Thermal discrepancies

## 9.4 Conclusions

In this article, we have observed effects on the thermal field of disturbances caused by intrusive instrumentation. We have carried out this study because of the failure of the equivalent heat source estimation for the case of “T” welding. Despite several assumptions, our direct problem has been confirmed thanks to macrographies. However, this validation is not significant because it compares a simulated fused zone to a maximal weld pool size observed on the transversal plan. This led us to apply an inverse method which makes 3D temperature comparisons. But, theoretical estimations were made before the implementation of experimental case. This for two reasons, firstly, sensitivity amplitudes and independences have been checked, and secondly, an artificial measurement noise has been added to theoretical temperature acquisition, this in order to check the estimation capacity without a perfect signal. In these two cases, results have been very satisfactory so we have validated thermocouple location and defined an a priori instrumentation.

Nevertheless, the inverse problem with real information has failed, and thus after experimental result analysis, thermal measurement has been selected as the most important origin of disturbances. Consequently, to observe thermocouple effects, we have chosen to simulate two kinds of them, first, with laboratory shape and secondly, with industrial characteristics. Moreover, two implementation methods have been studied, the first respects the thermocouple measurement theory by being inserted parallel to isothermal surfaces, the second is our experimental case, imposed by industrial requirement, and in which the hole is made perpendicular to isotherms. Results of this analysis are very interesting and help explain our experimental errors. We have shown that a laboratory thermocouple inserted along the thermal flow direction stops the diffusion and induces a thermal accumulation at the end of the hole where the measurement is made. Conversely, when it is perpendicular to the flow, the thermocouple has a temperature which is very close to the undisturbed one and this throughout the time. The link between this cause of error and experimental temperature discrepancies are thus made. After, we have tried to simulate the industrial thermocouple, those with sheath. In this case, perfect contact conditions are difficult to be obtained, so a thermal contact resistance has been assumed. Also in this part, simulation has explained some experimental errors, for example, discrepancies between two thermocouples at the same coordinates could result from the bad contact of one over the workpiece.

Finally, this instrumentation simulation has shown why an inverse problem, with a non-optimal experimental implementation, does not find satisfactory results. So it is possible to define an implementation method which limits temperature disturbances but increases estimation sensitivities.

Measurements had to be realized:

- all around the weld pool,
- as close as possible to the fused zone,
- in such a way as to observe thermal gradient (for example: along two lines),
- in holes drilled perpendicular to the heat flow,
- with the best contact quality.

But when this recommendation cannot be applied two solutions exist. The first is the use of a direct problem which simulates the whole instrumentation inside the workpiece. But the shape of thermocouples induces a very thin mesh and current computing resources do not allow for this level of simulation. The second is the development of an error model that can be applied on direct problem measurements; this will be the next part of our study.

## 9.5 References

- [1] Ecole d’Hiver – METTI 99, “Métrologie thermique et Techniques inverses”, 25-30 janvier, Odeillo Font Romeu, Vol. 1 and 2, Presses Universitaires de Perpignan 1999.
- [2] Beck J.V., Arnold K.J., “Parameter estimation in engineering and science”, Wiley, New York, 1977
- [3] Bardon J.P., Cassagne B. “Température de surface: mesures par contact” Techniques de l’Ingénieur, Paris R2732, 1-22, 1981

- [4] Cassagne B., Kirsch G, Bardon J.P. “Analyse théorique des erreurs liées aux transferts de chaleur”, Int. J. of Heat Mass Transfert, vol. 23, pp 1207-1217, 1980.
- [5] Géry A., Thèse de doctorat, Lyon, Avril 1980
- [6] Werling E., Thèse de doctorat, INSA de Lyon, Janvier 1988
- [7] Bouvier A., Thèse de 3ième cycle, Université de Nantes, 1986
- [8] Le Masson P., « Etude d’une méthode de mesure des transferts convectifs entre un écoulement à grande vitesse et les parois d’un canal de très petites dimensions utilisant des techniques inverses et des microthermocouples semi-intrinsèques », Thèse de doctorat, Université de Nantes, 1991
- [9] Cassagne B., Bardon J.P., Beck J.V., “Theoretical and experimental analysis of two surface thermocouples”, Proceeding of 8<sup>th</sup> Int. Heat Transfer Conf., Vol. 2, pp 483-488, 1986
- [10] MUSICA Project:  
[http://www.cea.fr/le\\_cea/actualites/le\\_cea\\_areva\\_le\\_cetim\\_et\\_la\\_societe\\_esi\\_grou-2699](http://www.cea.fr/le_cea/actualites/le_cea_areva_le_cetim_et_la_societe_esi_grou-2699)
- [11] S. Rouquette, J. Guo and P. Le Masson, “Estimation of the parameters of a Gaussian heat source by the Levenberg-Marquardt method : Application to the Electron Beam Welding”, article accepté après corrections dans International Journal of Thermal Sciences (2006).
- [12] J. Guo, P. Le Masson, E. Artioukhine, T. Loulou, P. Rogeon, D. Carron, M. Dumons, J. Costa, « Estimation of a source term in a two-dimensional heat transfer problem : application to an electron beam welding », Inverse Problems in Engineering, vol.14 n°1, janvier 2006, pp. 21-38.
- [13] J. Goldak, M. Bibby and A. Chakravarti, International Institute of Welding, Volumes 603-685, 1985.
- [14] D. Li and M.A. Wells, Metallurgical and Materials T